

## Dynamics of Magnetic Domain Wall Motion after Nucleation: Dependence on the Wall Energy

K. Fukumoto,<sup>1,\*</sup> W. Kuch,<sup>1</sup> J. Vogel,<sup>2</sup> F. Romanens,<sup>2</sup> S. Pizzini,<sup>2</sup> J. Camarero,<sup>3</sup> M. Bonfim,<sup>4</sup> and J. Kirschner<sup>5</sup>

<sup>1</sup>*Institut für Experimentalphysik, Freie Universität Berlin, Arnimallee 14, D-14195 Berlin, Germany*

<sup>2</sup>*Laboratoire Louis Néel, CNRS, 25 avenue des Martyrs, B. P. 166, F-38042 Grenoble cedex 9, France*

<sup>3</sup>*Departamento de Física de la Materia Condensada, Universidad Autónoma de Madrid, E-28049 Madrid, Spain*

<sup>4</sup>*Departamento de Engenharia Elétrica, Universidade do Paraná, CEP 81531-990, Curitiba, Brazil*

<sup>5</sup>*Max-Planck-Institut für Mikrostrukturphysik, Weinberg 2, D-06120 Halle, Germany*

(Received 26 September 2005; published 9 March 2006)

The dynamics of magnetic domain wall motion in the FeNi layer of a FeNi/Al<sub>2</sub>O<sub>3</sub>/Co trilayer has been investigated by a combination of x-ray magnetic circular dichroism, photoelectron emission microscopy, and a stroboscopic pump-probe technique. The nucleation of domains and subsequent expansion by domain wall motion in the FeNi layer during nanosecond-long magnetic field pulses was observed in the viscous regime up to the Walker limit field. We attribute an observed delay of domain expansion to the influence of the domain wall energy that acts against the domain expansion and that plays an important role when domains are small.

DOI: [10.1103/PhysRevLett.96.097204](https://doi.org/10.1103/PhysRevLett.96.097204)

PACS numbers: 75.60.Jk, 75.50.Bb, 75.60.Ch, 75.70.Kw

Many of the fascinating phenomena in thin film magnetism that appear promising for new applications in magnetic data storage involve the use of multilayered magnetic systems, for example, spin valves [1] and magnetic-tunnel junctions [2]. The study of the time dependence of the magnetic properties in multilayered systems is of high actual interest with respect to the achievable magnetic response time of such devices, but also from a fundamental point of view. It has been observed that the magnetization reversal for hard-soft magnetic trilayers is dominated by domain wall motion in quasistatic conditions and by the nucleation of many small domains in fast dynamic conditions [3,4]. Such a difference in the reversal mechanism must obviously be accompanied by dramatic changes in the energetics, and magnetic domain walls will become much more influential at faster reversal rates.

The role of domain wall energy on the magnetization reversal is a long-debated issue. It has been discussed in the 1970s in connection with bubble domains in perpendicularly magnetized materials. Malozemoff and Slonczewski pointed out that the domain wall energy leads to a wall curvature pressure that tends to contract an isolated bubble domain, eventually collapsing the domain when the opposing demagnetizing energy is overcome [5]. Skomski *et al.*, in a self-consistent magnetic-viscosity approach, pointed out a negative velocity for bubble domain expansion in small fields as consequence of the domain wall energy, thus confirming the domain collapse [6]. More recently, Lyberatos and Ferré studied the rate of domain growth in an applied magnetic field by Monte Carlo simulations. The results showed a slowing down of domain wall motion and the appearance of a fractal shape of the domains due to pinning effects in the regime of thermally activated domain wall motion. However, no influence of domain wall energy was found in the viscous motion regime, in which pinning processes do not hinder the domain wall propagation [7].

Experimentally, it has been shown that the influence of the domain wall energy can lead to a straightening of domain walls in the low velocity creeplike motion regime in the presence of an introduced defect [8], and to a selectively accelerated domain expansion of such wall motion processes leading to a merging of domains [9].

In this Letter we present an experimental investigation of the influence of the domain wall energy on the magnetization reversal of the soft magnetic layer in magnetic tunnel junction-like trilayers. We study the reversal of the soft layer away from the magnetization direction of the hard layer. In this configuration the reversal is nucleation-dominated for high fields [3,4], and a strong influence of the domain wall energy is expected. We use a stroboscopic pump-probe technique [10] to observe in real space the repeated nucleation and expansion of domains and find that the influence of the domain wall energy leads to an apparent delay in domain nucleation, which can amount up to several nanoseconds. This can be well described by an effective specific domain wall energy exerting a negative domain wall pressure when domains are small, just after nucleation, but becoming negligible once domains exceed a certain size.

In in-plane domains there is no stabilizing demagnetizing energy as in perpendicular bubble domains, and the domain wall energy  $P\gamma d$  of a domain with perimeter length  $P$  in a film of thickness  $d$  [6] can be described simply by an effective field  $H_{\text{wall}} = \gamma\lambda/(4\mu_0 M_S P)$  acting against the external field  $H_{\text{ext}}$  [5]. Here  $\gamma$  is an effective domain wall energy averaged over the perimeter of the domain, and  $\lambda$  is a geometric factor describing the ratio between area and squared perimeter of the domain ( $\lambda = 4\pi$  for a circular domain). Only if  $H_{\text{wall}}$  is small enough so that the corresponding wall velocity can be neglected, domains are stable in static conditions. In our case, both the domain wall field and the effective field from the

coupling between the two ferromagnetic layers in a trilayered structure,  $H_{\text{copl}}$ , oppose the externally applied field, so that the total effective field is

$$H_{\text{tot}} = H_{\text{ext}} - H_{\text{copl}} - \frac{\gamma\lambda}{4\mu_0 M_S P}, \quad (1)$$

and thus depends on  $P$ . We consider as measurable quantity the speed of perimeter expansion,  $dP/dt$ , which in turn will be a function of  $H_{\text{tot}}$ . We show that the resulting inhomogeneous nonlinear differential equation for  $P$  can well describe the observed apparent delay in reversible domain nucleation using a fixed value for  $\gamma\lambda$ , thus revealing the manifestation of the domain wall energy in the reversal dynamics.

The sample used in this study was a 4 nm  $\text{Fe}_{20}\text{Ni}_{80}$ /2.6 nm  $\text{Al}_2\text{O}_3$ /7 nm Co trilayer grown by rf sputtering on the step-bunched surface of a  $6^\circ$  miscut Si(111) crystal. Underneath the Co layer, 3 nm of CoO has been deposited to increase the coercivity of the Co layer. The FeNi layer has been capped by 3 nm of Al to prevent oxidation. Details of the thermal treatment leading to the creation of step bunches are given in Ref. [11]. According to quasistatic longitudinal Kerr effect experiments, the sample features uniaxial anisotropy along the step bunches. The coercivities are 1 mT for the FeNi and 4.3 mT for the Co layers, and a Néel type coupling field  $\mu_0 H_{\text{copl}}$  of 1.2 mT favors parallel alignment. Details of similar types of samples are shown in Refs. [3,4,9,10,12].

The experiment was performed using a combination of x-ray magnetic circular dichroism (XMCD), photoelectron emission microscopy (PEEM), and a stroboscopic pump-probe technique [10]. Magnetic field pulses are periodically applied at 312.5 kHz by a coil made of Cu foil wrapped around the sample. The magnetic response is stroboscopically probed by XMCD-PEEM with the same frequency at a fixed phase delay with respect to the magnetic field pulses. The time resolution is given by the x-ray pulse width and the jitter of the electronics, and is estimated as 100 ps. The domain wall motion in the two ferromagnetic (FM) layers was observed separately by tuning the photon energy of circularly polarized x rays to the Fe and Co  $L_3$  absorption edges for addressing the FeNi and Co layer, respectively. Measurements were performed at the UE56/2-PGM2 beam line at BESSY in Berlin.

In Fig. 1 we show images of the nucleation of domains and their subsequent expansion in the FeNi layer, observed at an amplitude of the bipolar field pulses of 5.8 mT. The pulse shape is shown in Fig. 1(e). The positive and negative parts have the same amplitude (5.8 mT) and length (47 ns). Figures 1(a)–1(d) show the magnetic domain structures in the FeNi layer at different pump-probe delay times, 9, 19, 24, and 29 ns, respectively. The easy axis is parallel to the vertical direction in the images, and the black and white contrasts indicate the magnetization pointing down and up, respectively. The direction of the incoming x rays with  $30^\circ$

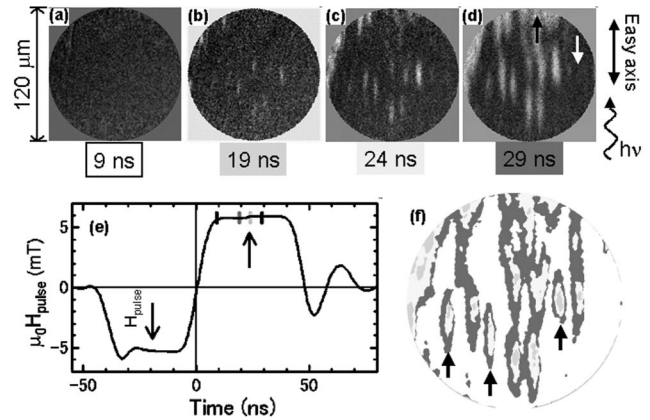


FIG. 1. Bipolar magnetic field pulses (e) were used to reverse the magnetization in part of the FeNi layer. The amplitude of the field pulses was 5.80 mT on the plateaus of both the positive and negative part of the pulses. The magnetic domain structure in the FeNi layer at different delay times is shown in (a)–(d), where the photon energy of circularly polarized x rays was tuned to the Fe  $L_3$  absorption edge. White domains in (b) to (d) are discretized and superimposed to (f). Different shades of gray in (f) indicate different delay times. Images taken at the Co- $L_3$  edge confirmed that no magnetization changes took place in the Co layer.

grazing angle to the surface is also indicated in Fig. 1(d). The field of view is  $120 \mu\text{m}$ .

Before applying the pulses, the two FM layers were magnetically saturated in the same direction by a 15 mT field pulse of 3 ms duration. The direction is indicated by the white arrow in Fig. 1(d), and corresponds to black contrast. During the pump-probe experiments, the first, negative part of the pulse is in the same direction as the saturation, and was used to obtain the same starting condition for each pulse. The second, positive part is in the opposite direction [see Fig. 1(e)]. The magnetization in the FeNi layer starts to reverse into the white direction during this second part of the pulse. The start of the positive part of the pulse is set to zero time. The plateau of the pulse starts at 9 ns, at which time one can see only some small fuzzy white splotches, probably due to magnetic domains that are blocked on surface defects [Fig. 1(a)]. However, they do not expand with time, and are thus not regarded in the analysis. Some white domains become visible in Fig. 1(b), and, as time goes by, they get larger [Fig. 1(c) and 1(d)]. To get sufficient statistics, millions of pulses were applied to acquire each image.

The areas of white domains in Figs. 1(b)–1(d) are superimposed into Fig. 1(f) with different shades of gray, middle gray, light gray, and dark gray, respectively. The expansion of the domains by propagation of the domain walls is clearly seen. In this experiment, the magnetization of the Co layer was not affected by the field pulses; i.e., it always showed the black contrast.

In Fig. 2, the average perimeter of the three domains indicated by arrows in Fig. 1(f) is plotted as a function of

time for each amplitude  $H_{\text{pulse}}$  of the field.  $\mu_0 H_{\text{ext}}$  is ranging from 5.62 to 6.81 mT. The perimeter  $P$  is measured by an ellipse fit to the domains with an error of about 10%. The three domains were nucleated for all amplitudes of the field pulses, and it was possible to measure  $P$  before they merged with other surrounding domains. The start of the plateau is indicated by a vertical line in Fig. 2. Linear fits to the data (broken lines) indicate that the measured values for  $P$  extended linearly with time for each field amplitude. However, the intersections to the time axis of these lines do not come to the same point, but show an apparent delay in the appearance of the domains, which amounts up to 17 ns for  $H_{\text{ext}} = 5.62$  mT.

In Fig. 3, the slope of linear fits to the experimental data of Fig. 2, i.e., the speed of perimeter expansion for large domains, is plotted versus  $\mu_0 H_{\text{ext}}$  (bottom axis) and versus  $\mu_0(H_{\text{ext}} - H_{\text{copl}})$  (top axis). In the range of  $\mu_0 H_{\text{ext}}$  between 5.6 and 6.4 mT,  $dP/dt$  increases linearly with field, meaning that the wall motion is in the viscous regime in this field range. A mobility of *perimeter extension*,  $\mu$ , of  $7800 \text{ m}/(\text{s mT}) \pm 10\%$ , was obtained from the slope of a linear fit. The two data points with the highest amplitudes of the field pulses (6.70 mT and 6.81 mT) are not included in the linear fit, since the velocity seems to reach saturation at around 5.2 mT of  $\mu_0(H_{\text{ext}} - H_{\text{copl}})$ . This saturation of velocity is due to the modification of the spin structure inside the domain wall above the so-called Walker limit field [13,14].

For the analysis according to Eq. (1) we use the data of Fig. 3 to extract the dependence of  $dP/dt$  on  $H_{\text{tot}}$ , where we assume  $H_{\text{tot}} \approx H_{\text{ext}} - H_{\text{copl}}$  for large domains. The negative contribution of  $H_{\text{wall}}$  to  $H_{\text{tot}}$  for small domains makes it necessary to extend the velocity data to the lower field range for the numerical evaluation of  $P(t)$ . We assumed thermally activated wall motion for lower  $H_{\text{tot}}$  with perimeter extension velocity

$$v_P = v_{P,0} \exp\left(\frac{\mu_0 M_S H_{\text{tot}} V_B - E_p}{k_B T}\right), \quad (2)$$

where  $V_B$  and  $E_p$  are the Barkhausen volume and the barrier energy, respectively [15,16], and  $\mu_0 M_S = 1 \text{ T}$  for FeNi. To provide a smooth transition to the experimentally determined regime of viscous motion at  $H^* = 4.4 \text{ mT}$ , values of  $V_B = (1.2 \pm 0.1) \times 10^{-23} \text{ m}^3$  and  $E_p = (2.6 \pm 0.4) \times 10^{-20} \text{ J}$  [3] have to be used (solid line in Fig. 3), while  $v_{P,0} = 55 \text{ nm/ns}$  [17]. At  $H_{\text{tot}} > 5.2 \text{ mT}$ , a constant perimeter expansion speed of  $9.3 \text{ } \mu\text{m/ns}$  was assumed in order to match the two data points at 6.70 and 6.81 mT.

The perimeter extension was numerically evaluated according to Eq. (1) with 1 ps time increments [18] and is plotted in Fig. 2 by solid curves. The best agreement was obtained for  $P(t=0) = 1.9 \text{ } \mu\text{m}$  and  $\gamma\lambda = 9 \text{ mJ/m}^2$ . The simulation fits quite well to the experimental data.  $P(t=0)$  and  $\gamma\lambda$  are found to be correlated by  $\gamma\lambda = 3 \times 10^4 (\text{mJ/m}^3) P(t=0) + 3.2 (\text{mJ/m}^2)$ , and no significant worsening of the fit is observed for values of  $\gamma\lambda$  between 7 and  $11 \text{ mJ/m}^2$ , if  $P(t=0)$  is changed accordingly and kept within 3% of the respective value. It is seen that a deviation from the linear behavior occurs at the initial stages of domain expansion, thus leading to the observed apparent delay. For higher  $\mu_0 H_{\text{ext}}$  (6.70 mT and 6.81 mT),  $P$  starts to expand already on the rising slope of the pulse before 9 ns, as was also observed in the experiment.

The above simulation assumed that there is no real delay in domain nucleation. Since the gray scale contrasts obtained in a static experiment were identical to the ones of the images obtained in the above experiment, the reproducibility of domain nucleation is close to 100%. Once the domains were visible, we did not observe an increase of the number of domains during the field pulses. This indicates that the domains were always nucleated as soon as the

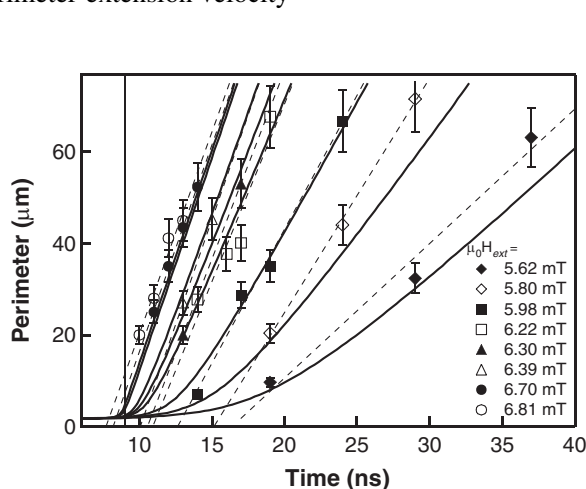


FIG. 2. Increase of the domain perimeter vs time during the plateau of the positive part of the field pulses for several field amplitudes. Broken lines are linear fits to the data. A simulation of the perimeter extension with time is shown by solid curves.

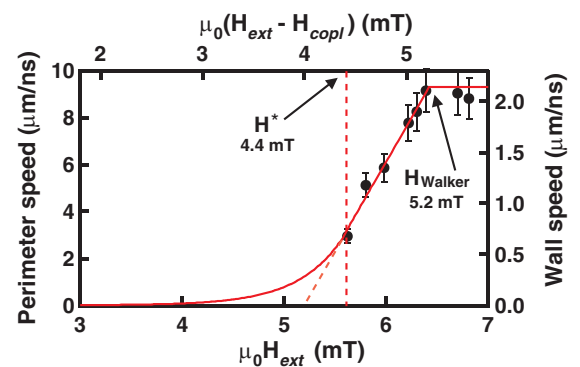


FIG. 3 (color online). Speed of perimeter extension vs  $\mu_0 H_{\text{ext}}$  (bottom axis) and  $\mu_0(H_{\text{ext}} - H_{\text{copl}})$  (top axis). The linear fit to six of the data points ranging from 4.4 mT to 5.2 mT of  $\mu_0(H_{\text{ext}} - H_{\text{copl}})$  indicates that the extension of the perimeter (i.e., the wall motion) is in the viscous regime. The exponential part at lower fields [ $\mu_0(H_{\text{ext}} - H_{\text{copl}}) < 4.4 \text{ mT}$ ] is drawn using Eq. (2). In the higher field region, above  $H_{\text{Walker}}$ , the perimeter speed is assumed to be constant ( $9.3 \text{ } \mu\text{m/ns}$ ).

pulse field reached a certain threshold. The observation of a reproducible nucleation of domains at certain locations of the sample means that topographic features act as nucleation centers, and that the nucleation process is not thermally activated. Reproducible nucleation takes place at those positions where the local nucleation barrier is lower than the effective field. The increase of the number of nucleated domains with increasing pulse height indicates therefore a distribution of barrier heights.

We have assumed a constant elliptical shape for the domains with aspect ratio 1:4, thus  $\lambda \approx 24$ . The perimeter speed can be converted into a domain wall speed along the easy axis of magnetization. This is plotted on the right axis of Fig. 2. The mobility of viscous domain wall motion along the easy axis is then  $1600 \text{ m}/(\text{s mT}) \pm 10\%$ . The initial  $P$  of  $1.9 \mu\text{m}$  means that the width of the nucleation centers is around  $0.19 \mu\text{m}$ , which is too small to be seen in the images, the lateral resolution of which was set to  $\approx 1 \mu\text{m}$  for these measurements. The maximum speed of  $2000 \text{ m/s}$  along the easy axis is an order of magnitude larger than the value found for narrow permalloy lines using similar field values, indicating that it might be possible to increase this speed by an appropriate shaping of the wires [19].

The Walker limit field is given by  $\mu_0 H_{\text{Walker}} = 1/2\alpha\mu_0 M_S$  [13]. For  $\text{Fe}_{20}\text{Ni}_{80}$ , a value  $\alpha = 0.01$  is often used in the literature for the damping constant [4,20,21]. With this value,  $\mu_0 H_{\text{Walker}}$  would be  $5 \text{ mT}$ . This is in good agreement with our experimentally obtained value of  $5.2 \text{ mT}$ .

The constant effective domain wall energy  $\gamma = 0.38 \text{ mJ/m}^2$  that was used for the simulation includes exchange and anisotropy energy inside the wall, magneto-static contributions from the sharp ends of the elliptic domains, as well as repulsion of the long sections of the magnetic domain walls [22]. A refined model should take into account the dependence of  $\gamma$  on  $P$ . Since in the simulation  $\gamma$  contributes mainly when domains are small, deviations in the shape of the domains may also play a role when comparing the value for  $\gamma$  to an estimate for the wall energy of an isolated Néel type wall, which leads to a much higher value of  $2.3 \text{ mJ/m}^2$  [23].

In conclusion, the reproducible nucleation of domains in the soft layer of a tunnel junction-like trilayer and the subsequent domain growth by domain wall propagation in the viscous regime and up to the Walker limit field is significantly influenced by the energy of magnetic domain walls. This leads to an apparent delay of domain expansion. A faster magnetization reversal, which is required for the coming magnetic recording devices, is drastically hindered by this magnetic domain wall energy when magnetic domains are small. By analogy, the techniques and results shown in this work are equally applicable to other nuclea-

tion and growth phenomena like crystallographic phase changes, superconducting transitions, and solidification theory.

We thank F. Helbig, B. Zada, W. Mahler, and G. Meyer for technical support, F. Petroff and A. Vaurès for sample preparation. Financial support by BMBF (No. 05KS1EFA6), EU (BESSY-EC-HPRI Contract No. HPRI-1999-CT-00028), and Laboratoire Européen Associé (LEA) “Mesomag” is gratefully acknowledged.

---

\*Present address: JASRI/SPring-8, 1-1-1, Kouto, Sayo, Hyogo 679-5198, Japan.

- [1] J. M. George *et al.*, Phys. Rev. Lett. **72**, 408 (1994).
- [2] J. S. Moodera, L. R. Kinder, T. M. Wong, and R. Meservey, Phys. Rev. Lett. **74**, 3273 (1995).
- [3] Y. Pennec *et al.*, Phys. Rev. B **69**, 180402(R) (2004).
- [4] K. Fukumoto *et al.*, J. Magn. Magn. Mater. **293**, 863 (2005).
- [5] A. P. Malozemoff and J. C. Slonczewski, *Magnetic Domain Walls in Bubble Materials* (Academic, New York, 1979), Chap. 2.
- [6] R. Skomski, J. Giergiel, and J. Kirschner, IEEE Trans. Magn. **32**, 4576 (1996).
- [7] A. Lyberatos and J. Ferré, J. Phys. D: Appl. Phys. **33**, 1060 (2000).
- [8] L. Krusin-Elbaum *et al.*, Nature (London) **410**, 444 (2001).
- [9] W. Kuch *et al.*, Appl. Phys. Lett. **85**, 440 (2004).
- [10] J. Vogel *et al.*, Appl. Phys. Lett. **82**, 2299 (2003).
- [11] A. Encinas *et al.*, Appl. Phys. Lett. **71**, 3299 (1997).
- [12] J. Vogel *et al.*, Phys. Rev. B **72**, 220402(R) (2005).
- [13] N. L. Schryer and L. R. Walker, J. Appl. Phys. **45**, 5406 (1974).
- [14] S. W. Yuan and H. N. Bertram, Phys. Rev. B **44**, 12395 (1991).
- [15] J. Ferré, in *Spin Dynamics in Confined Magnetic Structures I*, edited by B. Hillebrands and K. Ounadjela (Springer, New York, 2002), p. 127.
- [16] A. Kirilyuk, J. Giergiel, J. Shen, and J. Kirschner, J. Magn. Magn. Mater. **159**, L27 (1996).
- [17]  $v_{P,0} \approx v_0 \sqrt{A_B}$ , where  $A_B$  is Barkhausen area, and  $v_0 = 10^9 \text{ s}^{-1}$ .
- [18] For the simulation, the pulse shape was simplified such that the field increases linearly with time during the rise time, the slope thus being  $\mu_0 H_{\text{ext}}/9 \text{ ns}$ . After  $9 \text{ ns}$ , the field is assumed constant up to the end of the plateau.
- [19] G. S. D. Beach *et al.*, Nat. Mater. **4**, 741 (2005); Y. Nakatani *et al.*, Nat. Mater. **2**, 521 (2003).
- [20] J. P. Nibarger, R. Lopusnik, Z. Celinski, and T. J. Silva, Appl. Phys. Lett. **83**, 93 (2003).
- [21] S. Ingvarsson *et al.*, Phys. Rev. B **66**, 214416 (2002).
- [22] A. Hubert and R. Schäfer, *Magnetic Domains* (Springer, New York, 1998), Chap. 3.6.4.
- [23]  $\sqrt{AM_S^2/(2\mu_0)} = 2.3 \text{ mJ/m}^2$  for  $A = 1.3 \times 10^{-11} \text{ J/m}$ .